

Synthesis of X-type zeolite and their influence on the filtration of dye effluents

Ayoub Tahiri^{a,*}, Abderrazek El-Kordy^a, Yassine Elyousfi^b, Lahcen Messaoudi^a,
Khalid Yamni^a, Najib Tijani^a, Mohamed Douma^a, Mohamed Messaoudi^a, Lotfi Rghioui^c

^aLaboratory of Materials, Membranes, and Nanotechnology, Department of Chemistry, Faculty of Sciences, Moulay Ismail University, PB 11201, Zitoune, Meknes, Morocco, Tel.: +212-658510069; emails: tahiriayoub15@gmail.com (A. Tahiri), abderrazekelkordy@gmail.com (A. El-Kordy) messaoudilahcen56@gmail.com (L. Messaoudi), k.yamni@umi.ac.ma (K. Yamni); najibtij@gmail.com (N. Tijani), m.douma@yahoo.fr (M. Douma), tmingenierie1@gmail.com (M. Messaoudi)

^bLaboratory Water and Environment Management, Department of Civil, Energy and Environment Engineering, ENSAH, Abdelmalek Essaadi University, Morocco, email: yassine.elyousfi@etu.uae.ac.ma

^cLaboratory of Spectroscopy, Molecular Modeling, Materials, Nanomaterials, Water and Environment, (LS3MN2E-CERNE2D), Department of Chemistry, Faculty of Sciences, Mohammed V University in Rabat, Morocco, email: rghiouilotfi@gmail.com

Received 12 June 2022; Accepted 17 December 2022

ABSTRACT

In the present study, a clay-based membrane support (m-S), and X-type zeolite, and a composite clay/zeolite membrane (m-ZX) were prepared. Membrane supports in the form of a flat-disc were prepared by uniaxial pressing of a mixture of clay and starch (12.0%, w/w starch/clay). The results of X-ray diffraction confirms the formation of X-type zeolite. While the scanning electron microscopy analysis shows the formation of fine particles with a crystal size between 1.47 and 2.08 μm with an octahedral shape. The nitrogen adsorption analysis showed that the specific surface area of the membrane support was $0.7655 \text{ m}^2\text{-g}^{-1}$ with an average pore diameter of 122.2 \AA . While the specific surface area of X-type zeolite was $316.95 \text{ m}^2\text{-g}^{-1}$ with an average pore diameter of 19.7127 \AA . The initial water permeation fluxes begin with valued of 1,018 and 380 $\text{Lm}^{-2}\text{-h}^{-1}$ for the membrane support (m-S) and the composite membrane (m-ZX), respectively. On the other hand, the filtration of the Eriochrome Black T (EBT) dye by m-S and m-ZX showed retention percentages of 38% and 69%, respectively. This clearly demonstrates the significant enhancement of retention of the dye on the m-ZX membrane. The points of zero charge (pzc) of the membrane support and X-type zeolite were $\text{pHpzc} = 8.77$ and $\text{pHpzc} = 10.2$, respectively. Filtration of the EBT dye was carried out at a pH of 8.2. This indicates that the membrane surface was positively charged while the EBT was negatively charged. The mechanism of the dye filtration was dominated by the size of the EBT molecule and that of the membrane pores, and also by the adsorption of the dye on the membrane due to the attraction between the negative charge of EBT and the positive charge on the membrane surface.

Keywords: X-type zeolite; Membrane; Clay; Retention; Eriochrome Black T

1. Introduction

Worldwide demand for colorful products in the industries, including all its categories namely textile, leather, plastic, cosmetics, paper and food, has seen an increase of 800,000 tons in consumption annually, with azo dyes

accounting for 60%–70% of the dyes used in the industry [1]. In view of the danger that may be caused by the damping of these dyes in water sources to ecosystems and on human health [2], in particular it may cause allergic disorders or hyperactivity in children and also different forms of cancer. These effluents must be treated before being released

* Corresponding author.

to the environment. The most common methods used for dye removal are coagulation–flocculation [3], photodegradation, oxidation [4], adsorption [5] and membrane filtration [6]. Among the anionic azo dyes, the Eriochrome Black T (EBT) (Fig. 1) is widely known, more than an indicator of metal ions, in the textile dyeing industry. Its toxic and carcinogenic properties have been the main characteristics for which EBT is the subject of several research for their elimination. Some important physico-chemical characteristics of EBT are molecular diameter $\varphi = 15.50 \text{ \AA}$, $\text{pK}_{a1} = 6.2$ and $\text{pK}_{a2} = 11.6$ at $T = 25^\circ\text{C}$ [7].

The membrane technology is one of the most attractive separation methods due to its low cost and high selectivity. Membrane filtration operations are common in the industry [8]. Membrane filtration is increasingly used as a separation process in many areas, particularly in the water cycle (purification of water, treatment of effluents, water reuse, softening and desalination, etc.). The principle of membrane filtration is based on the application of a pressure difference which allows the transfer of the solvent through a membrane whose pore size ensures the retention of solutes. Zeolite membranes have gained considerable attention over the last decade due to their interesting physicochemical properties such as uniform microporous structure, high thermal stability, mechanical resistance, and inertia to most chemical environments. Membranes are the subject of many applications, namely catalysis, pervaporation [9] metallurgical industry [10], separation of domestic and industrial wastewater treatment [11], and desalination of seawater [12]. In the present work, two membranes have been prepared; the first one is a clay-based named membrane support (m-S), and the second one is a composite clay/zeolite membrane named composite membrane (m-ZX), which is composed of the membrane support and a layer of zeolite deposited using the hydrothermal method for synthesis of X-type zeolite. The deposition of the zeolite layer was made on membrane supports based on clay that had a flat form. Starch was used as a porogen agent in the preparation of the membranes to ensure adequate porosity for filtration, with the presence of starch at 12% w/w of the clay-starch mixture [13]. To study the influence of the X-type zeolite layer on the ability of the membrane to remove a pollutant, filtration of the EBT dye in solution is carried out on both the membrane support and the composite membrane by measuring the flux and retention percentage of the dye.

2. Materials and methods

2.1. Chemicals and reagents

Sodium aluminate (NaAlO_2 , Sigma-Aldrich), sodium silicate (Na_2SiO_3 , Sigma-Aldrich), sodium hydroxide (NaOH , 99%, Merck), hydrochloric acid (HCl , 37%, Merck), sodium chloride (NaCl , >99.5%, VWR Chemicals BDH), starch ($\text{C}_6\text{H}_{10}\text{O}_5$) $_n$, Loba Chemie) and Eriochrome Black T ($\text{C}_{20}\text{H}_{12}\text{N}_3\text{O}_7\text{SNa}$, Loba Chemie). It should be noted that all these reagents are used without purification. In all experiments, Millipore deionized water with a resistance of $17.2 \text{ M}\Omega\cdot\text{cm}^{-1}$ was used. During zeolite synthesis, an autoclave and polypropylene bottles for the preparation of precursors based on silicates and aluminates were used.

2.2. Preparation of the membrane supports (m-S)

In this study, a clay extracted from the rif mountains of Morocco, precisely between the cities of Nador and Al-Hoceima ($35^\circ13'16.5''\text{N}$ $3^\circ35'37.2''\text{W}$) was used. The clay is then ground to fine particles and sieved using standard AFNOR sieves. Two ANFOR-standard sieves with mesh size of 80 and 160 μm were used to obtain clay particle sizes of $d < 80 \mu\text{m}$ and $80 < d < 160 \mu\text{m}$. The two particle sizes were used to prepare two membrane supports. The aforementioned were made with a mass fraction of 88 wt.% of the clay and the rest of the starch (12 wt.% by mass). The total mass of the sample was 4 g. The mixture was introduced to a stainless-steel die, and uniaxially pressed under a load pressure of 1,380 bars to obtain raw pellets (flat discs) 4.0 cm in diameter and 2.0 mm in thickness. The obtained discs are sintered to 950°C in a muffle furnace (type Nabertherm 2804) according to a heating program developed based on the thermal analysis of the raw clay.

2.3. Synthesis of X-type zeolite

In a polypropylene bottle, 0.035 mol of sodium aluminate and 0.01 mol of sodium hydroxide were placed, followed by 1.11 mol of distilled water heated to 60°C , the mixture was stirred until it becomes homogeneous. In other polypropylene bottle, 0.088 mol of sodium silicate were placed, followed by 2.77 mol of distilled water heated to 60°C , the mixture was stirred until it becomes homogeneous. Then the alumina precursor was added slowly to the silicate precursor under vigorous stirring. After the complete addition, the gel was left to age at room temperature for 30 min under vigorous stirring to obtain a homogeneous gel-mixture. Then it was transferred to a Teflon bottle, the latter being well sealed and placed in an air oven kept at a temperature of 100°C for 48 h. The products were then filtered, washed with water, and dried.

2.4. Preparation of the zeolite membrane by depositing of the X-type zeolite

The preparation of the m-ZX membrane is performed using a hydrothermal method. The clay-based membrane support sintered at 950°C was introduced into the Teflon bottle in a horizontal position, and then the gel previously

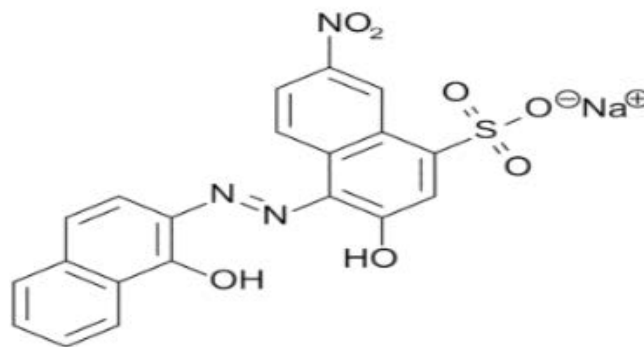


Fig. 1. Structure of Eriochrome Black T.

prepared was poured into the Teflon bottle. Then it is introduced into the oven for 48 h at a temperature of 100°C. Afterwards, the formed zeolite membrane is washed with distilled water and dried in an oven at a temperature of 60°C overnight [14].

2.5. Characterization techniques

In this work, several physical–chemical analysis techniques were used to characterize the clay and on the zeolite membrane, namely: X-ray fluorescence spectrometry in order to identify the elemental composition of the chosen clay and Fourier-transform infrared spectroscopy (FTIR) is carried out by dispersing clay and zeolite powders in KBr dried at 105°C and recorded on a JASCO – 4000 Fourier transform spectrometer in the range of 4,000–400 cm^{-1} . The X-ray diffraction (XRD) diffractograms of clay and zeolite were obtained using an X'PERT MPD-PRO type powder X-ray diffractometer (XRD) equipped with a diffracted beam monochromator and a Ni-filtered $\text{CuK}\alpha$ radiation source ($\lambda = 1.5418 \text{ \AA}$). The recording of X-ray diffraction data was done in a range of $2\theta = [2.5^\circ, 50^\circ]$ with a step increase of 0.02° and $t = 1 \text{ s/step}$ [15]. Differential thermal analysis (DTA) and thermogravimetric analysis (TGA) were conducted under air atmosphere and within a temperature range of 25°C–900°C, with a temperature increase of 10°C/min using SHIMADZU 60H apparatus. The need for thermal analysis lies in the information given about the material's behavior *vis-a-vis* temperature change, hence the importance of these results in the treatment and preparation of clay support. The Topcon EM 200B, equipped with energy-dispersive X-ray analysis (EDX) was used for detecting elemental analysis of micrographs scanned by scanning electron microscopy (SEM). This is to examine the morphology of the zeolite membrane and the

support on which it is deposited. Micromeritics ASAP 2010 is used to gain information about the textural characteristics of the material, exploiting nitrogen adsorption/desorption. Adsorption–desorption isotherms of N_2 were measured at 77.35 K, for the total pore volume was estimated at a pressure of about 0.96 bar. The resulting parameters are calculated using the Brunauer–Emmett–Teller (BET) theory and the Barrett–Joyner–Halenda (BJH) method, and the parameters obtained through this analysis are the total volume of the pores, the diameter of the pores and the size of the pores and the distribution of the pores, and the specific surface.

2.6. Point of zero charge

In a solution containing 100 mL of NaCl (0.001 M) and 1 mL of HCl (0.3 M), 0.2 g of the solid (X-type of zeolite or membrane support) was added. This mixture was stirred overnight, and another solution was prepared under the same conditions but without adding the solid (blank solution). The pH of the solutions was measured after each addition of a 50 μL volume of NaOH (0.3 M). In order to determine the pH_{pzc} , pH curves vs. the volume of NaOH were made. The pH_{pzc} is defined as the point of intersection between the curve of the studied solid and the curve of the blank solution [16].

2.7. Filtration flow loop

The filtration of the Eriochrome Black T dye was performed in a filtration system made in our laboratory, the components of which are illustrated in Fig. 2. This system consists of a feed container, a pump, control valves, pressure gauges for pressure control, and the filtration unit where the flat membrane is housed. The pressure is set to 1.0 bar,

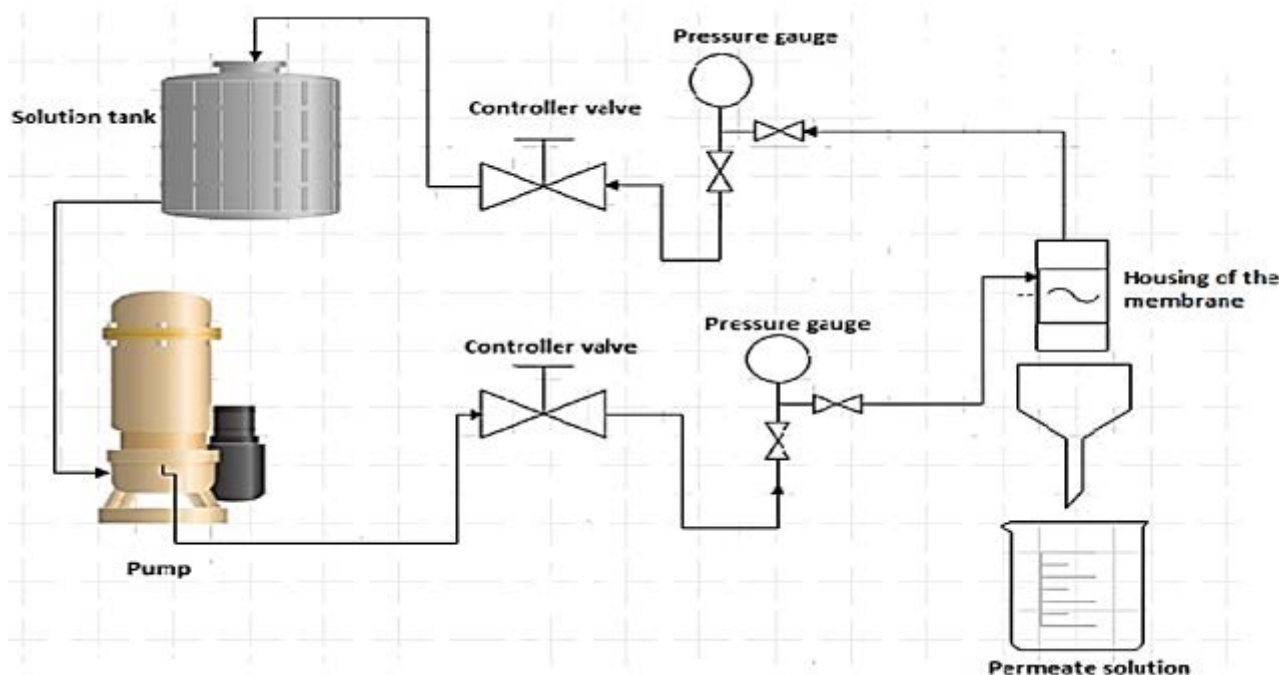


Fig. 2. Schematic representation of the frontal filtration system used at the scale of our laboratory.

the initial dye concentration was 10^{-4} M, the measured pH of the EBT stock solution was 8.2 (without any addition of other reagents), the filtration was done at room temperature (25°C), and the permeate was taken every 15 min. The samples have been analyzed by the Shimadzu UV-1240 to quantify the concentration of the dye in the permeate.

The performance of the synthesized membrane with or without a zeolite layer was assessed by the retention percentage of the dye used using Eqs. (1) and (2). Eq. (2) gives another parameter which corresponds to the flow rate, which is defined as the movement of a fluid through a given surface of the membrane for a period of time (t) [17].

$$\text{Retention}(\%) = \frac{C_0 - C_T}{C_0} \times 100 \quad (1)$$

In Eq. (1) C_0 is the molar concentration of Eriochrome Black T in the initial solution and C_T is the molar concentration in the permeate solution in a time.

$$\text{Rate Flux}(D) = \frac{V}{S \times t} \quad (2)$$

In Eq. (2) V is the volume of the permeate (L), S is the filtering surface (m^2) and t is the filtration time (h).

3. Results and discussion

3.1. X-ray diffraction analysis

The XRD analysis was done on raw and sintered clay at 550°C (to identify the presence of kaolinite) (Figs. 3 and 4). The diffractogram of the raw clay shows that the clay is made up of a mixture of phases. The identification of the different phases of the clay was made on the basis of the inter-reticular distances, the Miller indices, and position 2θ as follow: quartz 4.22, (100), 20.92°; 3.32, (101), 26.7°; 2.45, (110), 38.65°; 2.23, (111), 40.56°; 2.12, (200), 42.5°; 1.98, (021), 45.58°. Quartz diffractions were identified by powder diffraction file n° 96-900-5018. Kaolinite: 7.06, (001), 12.52°; 4.43, (020), 19.97°; 3.65, (002), 24.31°; 3.51, (112), 25.5°. Kaolinite diffractions have been identified via the powder diffraction

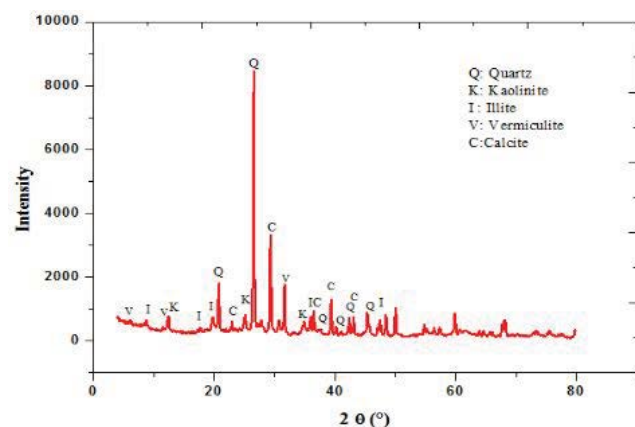


Fig. 3. XRD of the raw clay.

file n° 96-900-9231. Illite: 9.96, (002), 8.8°; 4.94, (004), 17.9°; 2.55, (-131), 35.06°; 1.87, (-134), 48.65°, illite diffractions were identified using a powder diffraction file 96-900-9666. Calcite: 3.84, (012), 23.13°; 3.02, (104), 29.5°; 2.48, (110), 36.17°; 2.27, (113), 39.5°; 2.08, (202), 43.29°, calcite diffractions were identified using a powder diffraction file 96-900-0096, Vermiculite: 14.11, (002), 6.14°; 7.03, (004), 12.29°; 3.52, (008), 25.35°, vermiculite diffractions were identified using a powder diffraction file 96-100-0037.

The diffractogram obtained from the X-ray diffraction analysis of the prepared X-type zeolite shows that it is indeed the desired phase, based on the characteristic peaks, in particular: 14.4, (111), 6.2°; 8.8, (220), 10.0°; 7.5, (311), 11.7°; 5.5, (331), 15.5°; 4.8, (511), 18.5°; 4.4, (440), 20.1°; 3.9, (620), 22.5°; 3.8, (533), 23.3°; 3.3, (642), 26.7°; 3.0, (733), 29.3°; 2.9, (822), 30.3°; 2.8, (555), 30.9° (Fig. 5). The indexing of the peaks was made on the basis of the data published by the international association of zeolite (IZA) and using the powder diffraction file 96-150-5694.

3.2. X-ray fluorescence analysis

Table 1 shows the X-ray fluorescence elemental analysis of the raw clay used in the preparation of the supports m-S. The major oxides observed in the sample are silicon, calcium, and aluminum, representing 72.95% of the overall composition of the clay. In addition, there are very low percentages of alkaline and alkaline-earth oxides (Na_2O , K_2O , and MgO). The presence of a large proportion of iron

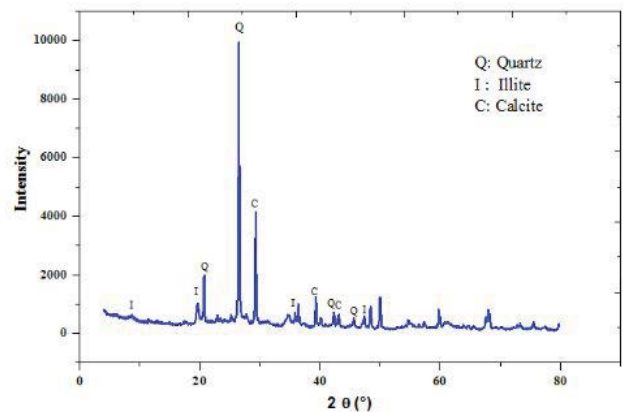


Fig. 4. XRD of the calcined clay at 550°C.

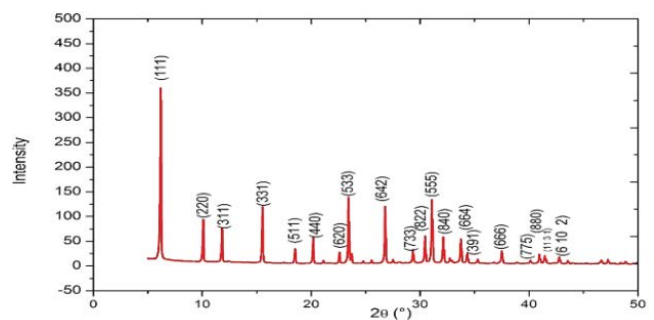


Fig. 5. XRD of the X-type zeolite.

oxide (5.43%) explains the appearance of the red coloration after heat treatment of the clay [18].

3.3. TGA/DTA analysis

The TGA curve in Fig. 6 shows that the clay has lost 18 wt.% (–2.443 mg) of its total mass during heat treatment between 25°C and 800°C. This total mass loss is due to the elimination of adsorbed water indicated by an intense peak around 84°C, the dehydroxylation of kaolinite and illite is indicated by a mass loss between 400°C and 700°C, and the decomposition of carbonates is found at a temperature of 768°C. Likewise, the DTA curve (Fig. 6) shows four endothermic peaks: two are intense peaks and two are of low intensity. These are responsible for the phenomena observed in the TGA analysis, namely the elimination of moisture from the water (intense peak at 84°C), dehydroxylation of kaolinite and illite (low intensity at 400°C and 531°C) and decomposition of carbonates (intense peak at 768°C) [19,20].

3.4. Infrared (FTIR) analysis

Fig. 7 shows the FTIR spectrum of the natural clay used in the preparation of the supports m-S. The recorded spectrum presents two bands of 3,643 and 3,482 cm^{-1} attributed respectively to OH stretching vibration of the Al–OH and Si–OH of the clay fractions and to the stretching vibration of the OH group from interstitial water between the

layers of the clay. The band of 1,680 cm^{-1} is attributed to the water adsorbed on the surface. The bands noted at 1,470 and 730 cm^{-1} are attributed, respectively, to the deformation and stretching vibrations of carbonates (CaCO_3). The band appeared at 1,025 cm^{-1} corresponds to the stretching (in-plane) vibration of the Si–O–Si bond [21]. The bands appearing at 490 and at 515 cm^{-1} are both attributed to the deformation vibrations of the Si–O bond [22].

Fig. 8 shows the FTIR spectrum of the prepared zeolite, characterized by a broad band at 3,440 cm^{-1} and a band at 1,650 cm^{-1} corresponding to OH stretching and bending vibration modes of the water molecules adsorbed by the zeolite, respectively. On the other hand, the band appearing at 1,001 cm^{-1} is attributed to the asymmetric stretching vibrations of the bridge bonds ν_{as} Si–O(Si) and ν_{as} Si–O(Al) [23]. Other significant bands were noticed at 554 and 665 cm^{-1} and they are attributed to symmetric stretching vibrations of bridge bonds ν_{s} Si–O–Si, and to symmetric stretching vibrations of bridge bonds ν_{s} Si–O–Al, respectively. The weak band observed at 462 cm^{-1} is attributed to internal vibrations of Si–O [24,25].

3.5. SEM analysis

SEM is used to examine the morphology of the surface and the shape of the crystals obtained, as well as the

Table 1
Oxides composition of the raw clay obtained by XRF analysis

Oxides	% mass
SiO_2	47.97
Al_2O_3	13.2
CaO	11.78
Fe_2O_3	5.43
MgO	2.42
K_2O	1.63
TiO_2	0.71
Na_2O	1.33
P_2O_5	0.09
Mn_2O_3	0.07
SO_3	0.44

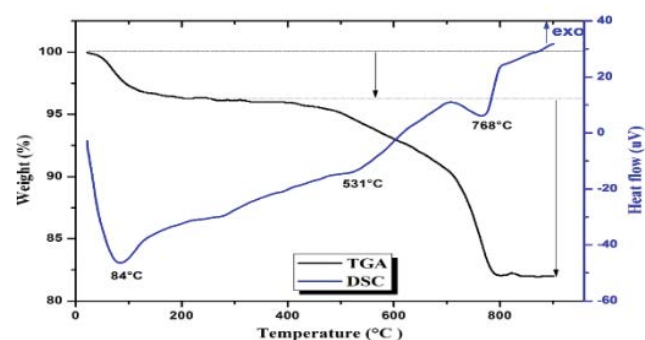


Fig. 6. TGA/DTA curves of the raw clay.

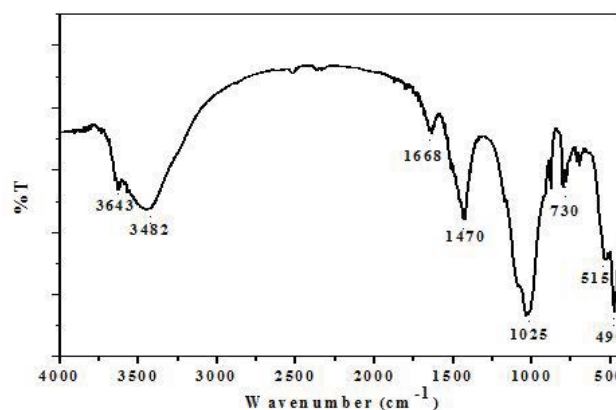


Fig. 7. Infrared analysis of the raw clay material used in the preparation of membrane support m-S.

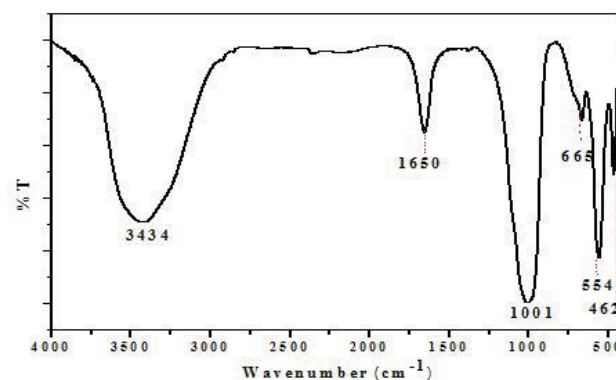


Fig. 8. Infrared analysis of X-type zeolite.

deposition of these crystals on the entire surface of the membrane support. Fig. 9 shows the selection of images under the SEM microscope coupled with EDX. The image in Fig. 9a is for the membrane support sintered at 950°C, Fig. 9c for the X-type zeolite powder, and Fig. 9d for the composite membrane.

The micrograph in Fig. 9a of the membrane support shows many pores with various sizes ranging from macro to micro sizes. It is also noted that the surface of the support is homogeneous and flawless because there are no agglomeration or cracks observed. The micrograph in Fig. 9c shows an SEM image of the X-type zeolite confirming the presence of small crystals of variable octahedral size between

1.47 and 2.08 μm . Fig. 9d represents the morphology of the zeolite membrane elaborated by the hydrothermal method. The presence of zeolite crystals was noticed inside the pores as well as on the surface of the flat disc supports [26].

The results of the semi-quantitative EDX analysis on the m-S membrane, X-type zeolite and m-ZX membrane are shown in the spectra presented in Fig. 9b, e and f, respectively. The percentages by weight of the oxides forming the prepared zeolite are as follows: silicon oxide (48.38%), aluminum oxide (35.76%), and sodium oxide (15.86%). On the other hand, the percentages by weight of the two chemical compositions of the m-S and m-ZX membranes clearly show the presence of silicon oxide (42.46%), aluminum oxide

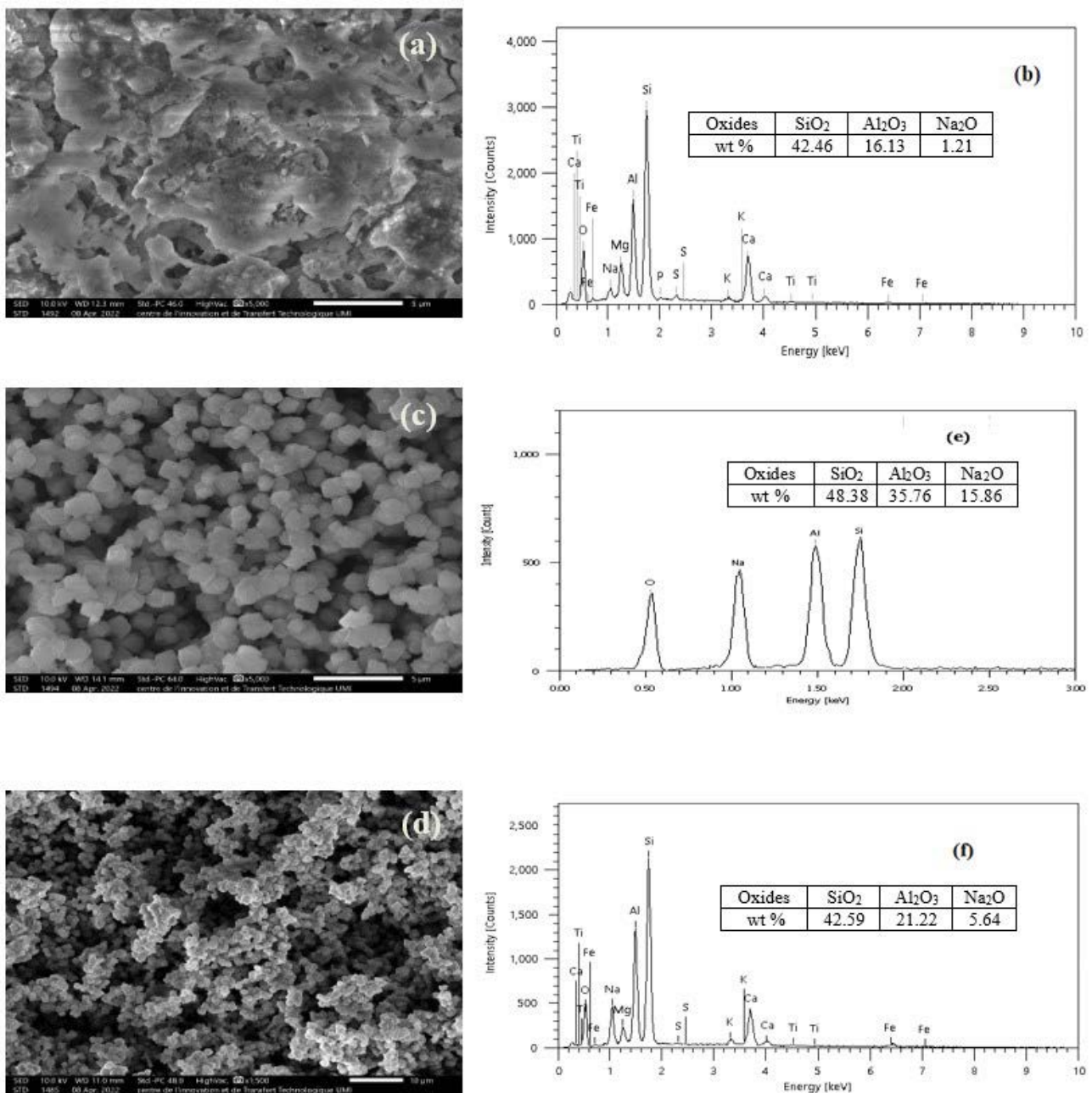


Fig. 9. SEM micrographs and EDX analysis of the clay support (a,b), X-type zeolite powder (c,e), and composite membrane (d,f).

(16.13%), and calcium oxide (23.73%) as the main elements for m-S, as well as silicon oxide (42.59%), aluminum oxide (21.22%), and sodium oxide (5.64%) as the main components of the m-ZX composite membrane. This shows that there is a significant increase in the weight percentages of silicon oxide, aluminum oxide, and sodium oxide in the m-ZX composite membrane compared to the m-S membrane support due to the deposition of the zeolite layer, in contrast, a reduction in the percentages of other oxides of Ca, Fe, and Mg.

3.6. Adsorption/desorption of nitrogen (N_2) analysis

Fig. 10 shows the nitrogen adsorption/desorption analysis of raw clay powder, the membrane support with $d < 80 \mu\text{m}$ and sintered at 950°C , X-type zeolite powder and m-ZX membrane. The adsorption/desorption parameters were obtained using the BET theory and the BJH algorithm. According to the IUPAC's hysteresis classification, the fundamental isotherms are classified as type IV with a d-Loop

and H_3 -type hysteresis. It is concluded from these results that these solids are mesoporous. In Table 2 are given the surface areas, the total pore volume and the pore diameter of the materials studied [27]. By Comparing the specific surfaces of the materials, the surface of the zeolite has a large surface area of $316.95 \text{ m}^2\cdot\text{g}^{-1}$ compared to the other materials. The surface decreases from 12.1751 to $0.7655 \text{ m}^2\cdot\text{g}^{-1}$ when moving from the clay powder to the membrane support because of the consolidation between the grains at 950°C . The same reasoning applies to the decrease in the total pore volumes from 0.030684 to $0.002960 \text{ cm}^3\cdot\text{g}^{-1}$ and the increase in pore diameters from 96.7859 to 122.1971 \AA . The surface of the m-ZX membrane was $3.3995 \text{ m}^2\cdot\text{g}^{-1}$, greater than that of the support ($0.7655 \text{ m}^2\cdot\text{g}^{-1}$), which is due to the deposition of the zeolite layer on the surface and in the pores of the support. The same reasoning applies to the increase in total pore volumes from the membrane support m-S to the composite membrane m-ZX, which have 0.002960 and $0.015226 \text{ cm}^3\cdot\text{g}^{-1}$, respectively. This indicates that the deposition of the

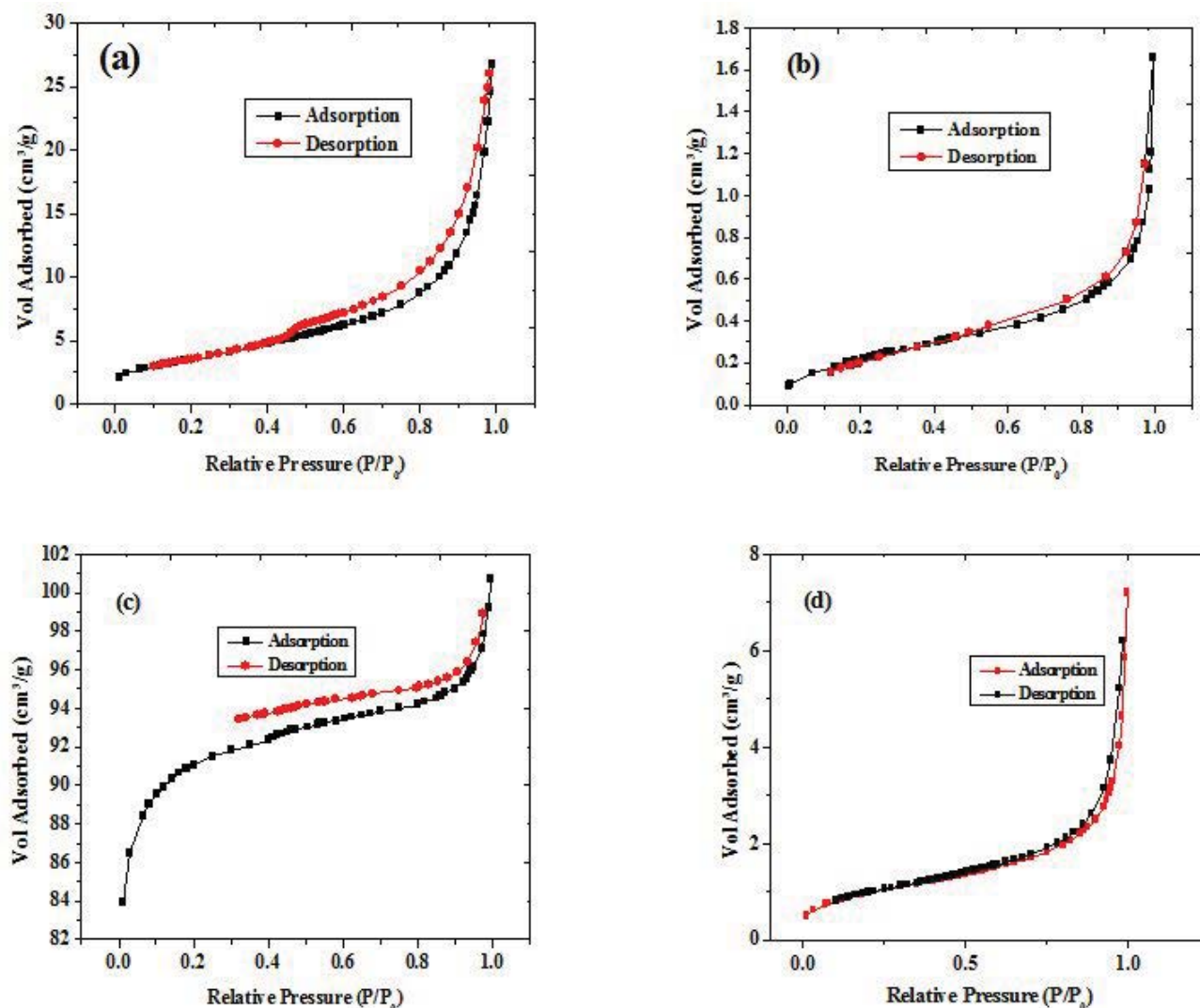


Fig. 10. Nitrogen sorption of raw clay (a), membrane support made from clay $d < 80 \mu\text{m}$ (b), and X-type zeolite powder (c), and m-ZX membrane (d).

zeolite on the support could further influence the filtration of the dye by reducing the size of the pores of the membrane support from 122.1971 to 68.9862 Å (Fig. 10).

3.7. Point of zero charge (PZC) of m-S and X-type zeolite

Since it provides information about the surface charge of the membrane, the pH of pzc (pHpzc) is a crucial parameter in membranes filtration, Fig. 11 shows the pHpzc of m-S and X-type zeolite. The curves represent the variation of pH vs. volume of NaOH added for the blank solution and the solution that contains the solid. The point of intersection between the curve of the solid analyzed with the curve of the blank solution corresponds to pHpzc. The pHpzc of m-S and X-type zeolite are 8.77 and 10.20, respectively. Therefore, the surface is negatively charged for higher pH values compared of pHpzc of the analyzed solid. While for pH below 8.77 and 10.20 the surface is positively charged for m-S and X-type zeolite, respectively. Since EBT filtration is greater in membranes which have positively surfaces. Because EBT filtration is more effective on membranes with positively charged surfaces, filtrations are carried out at a pH lower than the pHpzc of the two membranes. In addition, the pH of the dye solution measured during filtration were found to be around 8.20, so that the surfaces of m-S and zeolite are positively charged.

Table 2

Structural parameters of adsorption/desorption isotherms of N_2 on raw clay ($d < 80 \mu\text{m}$), membrane support, X-type zeolite (powder), and m-ZX membrane

Materials	S_{BET} ($\text{m}^2\cdot\text{g}^{-1}$)	V_p ($\text{cm}^3\cdot\text{g}^{-1}$)	d_p (Å)
Raw clay	12.1751	0.030684	96.7859
Membrane support	0.7655	0.002960	122.1971
X-type zeolite	316.9507	0.150153	19.7127
m-ZX membrane	3.3995	0.015226	68.9862

3.8. Calibration of the spectrophotometer UV/Vis for Eriochrome Black T

Fig. 12 represents the UV visible spectrum of the Eriochrome Black T solution, a characteristic band in the visible region located at 530 nm. This band was used for the determination of the corresponding concentrations of the permeates of the EBT dye. An external calibration curve of the spectrophotometer, is made using series of solutions of EBT dye ranging from 10^{-4} M to 10^{-5} M.

3.9. Water flux permeability for the clay support, membrane type-X zeolite

Water permeation tests were performed on clay supports with the two chosen granulometries ($80 \mu\text{m} < d < 160 \mu\text{m}$ and $d < 80 \mu\text{m}$) in order to select the appropriate granulometry and the most efficient support for the deposition of the zeolite layer.

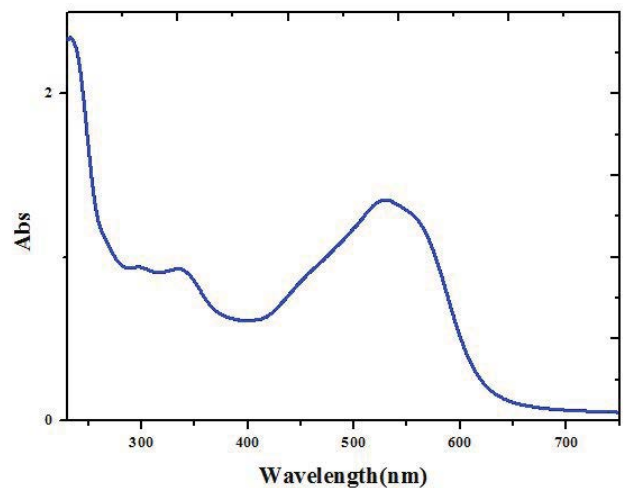


Fig. 12. UV-Vis absorption spectra of the EBT (pH = 8.2).

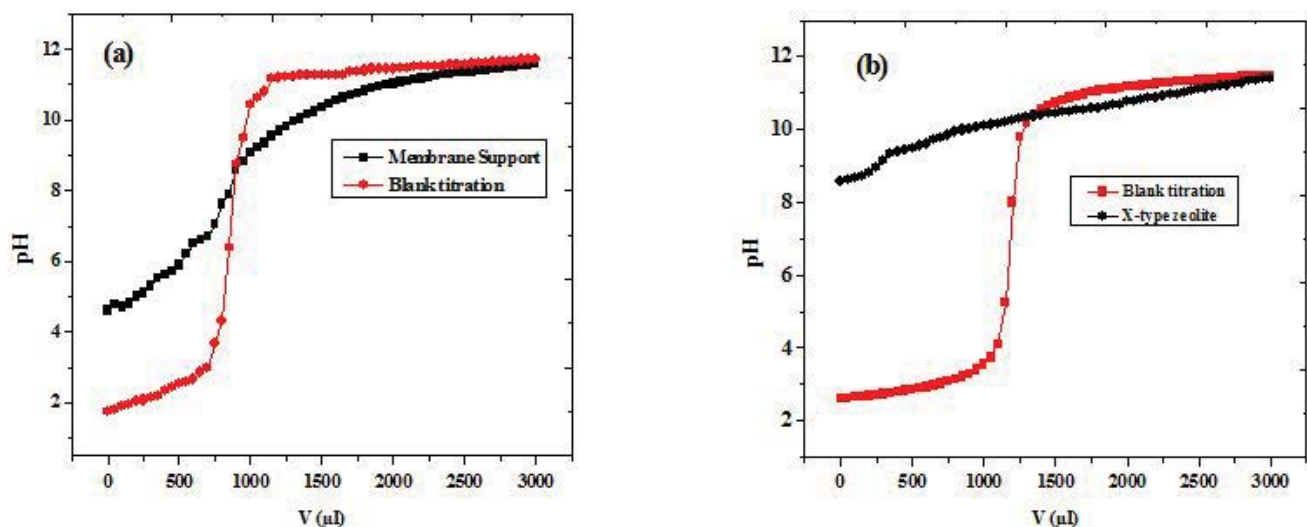


Fig. 11. pHpzc of membrane support m-S (a) and X-type zeolite powder (b).

Fig. 13a depicts the fluxes of the two supports as a function of time. After 15 min, the fluxes of the supports begin with the values of 1,018 and 1,272 $\text{Lm}^{-2}\cdot\text{h}^{-1}$. For supports of $d < 80 \mu\text{m}$ and $80 \mu\text{m} < d < 160 \mu\text{m}$ the values decrease as a function of time until reaching the values of 424 and 480 $\text{Lm}^{-2}\cdot\text{h}^{-1}$, respectively. After 3 h, the fluxes are almost stable, and final values of 410 and 471 $\text{Lm}^{-2}\cdot\text{h}^{-1}$ are obtained for supports $d < 80 \mu\text{m}$ and $80 \mu\text{m} < d < 160 \mu\text{m}$, respectively. It is concluded that the support made from clay powder of granulometry less than $80 \mu\text{m}$ can be considered as the most suitable for filtration because the other support has a remarkable high permeation of water, resulting in large pores, which makes the membrane less efficient for filtration.

Fig. 13b shows the water flux on the membrane composed of the clay-based support and the layer of X-type zeolite. The result of the test shows that the flux decreases

as a function of time, from which it begins with a value of $380 \text{Lm}^{-2}\cdot\text{h}^{-1}$ and, after 3.5 h, it reaches a value of $240 \text{Lm}^{-2}\cdot\text{h}^{-1}$.

By comparing the water flux obtained with the clay support and that obtained with the m-ZX membrane, the latter has an extraordinary effect; its flux is reduced by about 3 times compared to the clay support made from grains with diameter less than $80 \mu\text{m}$. This implies that the deposition of the zeolite has an important role in reducing the pore size of the support.

3.10. Filtration through m-S with and m-ZX membrane ($d \leq 80 \mu\text{m}$)

The performance of the membrane in relation to the filtration of the EBT dye has been studied in order to reinforce the results obtained with regard to the filtration of water

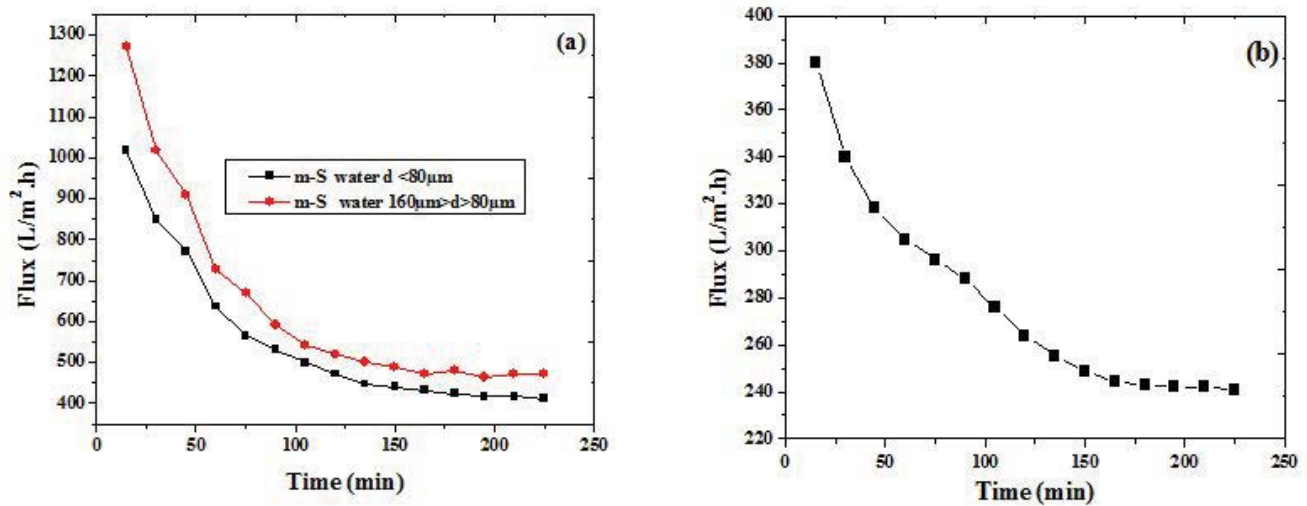


Fig. 13. Water flux variation vs. filtration time for the two supports made from $d \leq 80 \mu\text{m}$ (a) and $80 \mu\text{m} \leq d \leq 160 \mu\text{m}$ granulometries, composite membrane (m-ZX) (b) ($d \leq 80 \mu\text{m}$, $P = 1 \text{ bar}$).

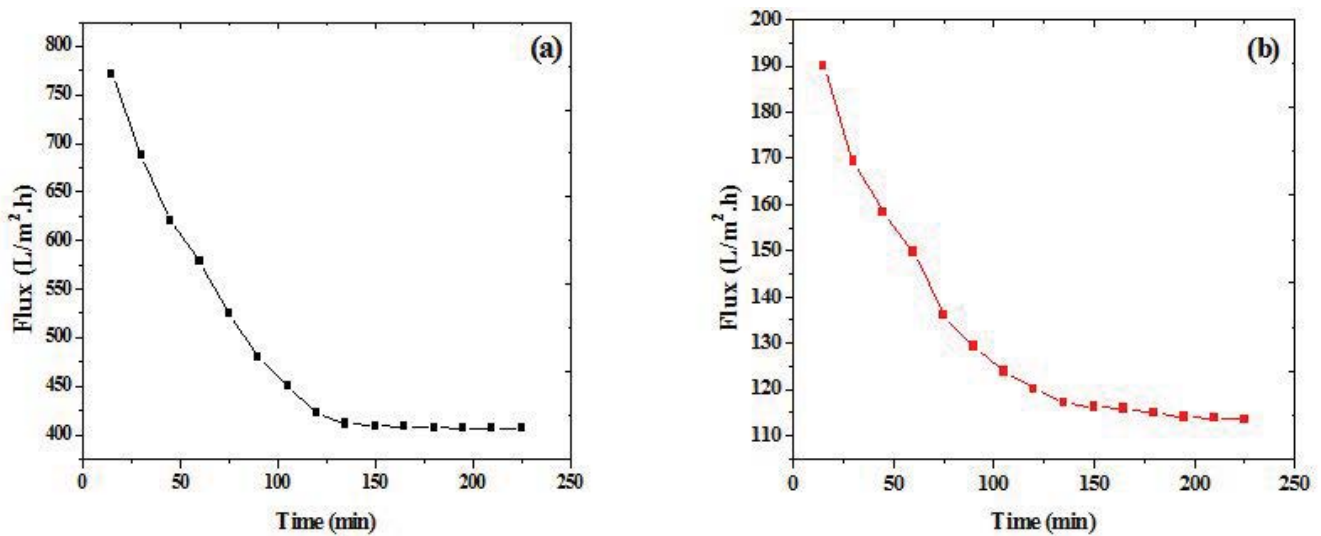


Fig. 14. EBT flux variation vs. filtration time for m-S (a) and m-ZX membrane (b) ($d \leq 80 \mu\text{m}$, $P = 1 \text{ bar}$).

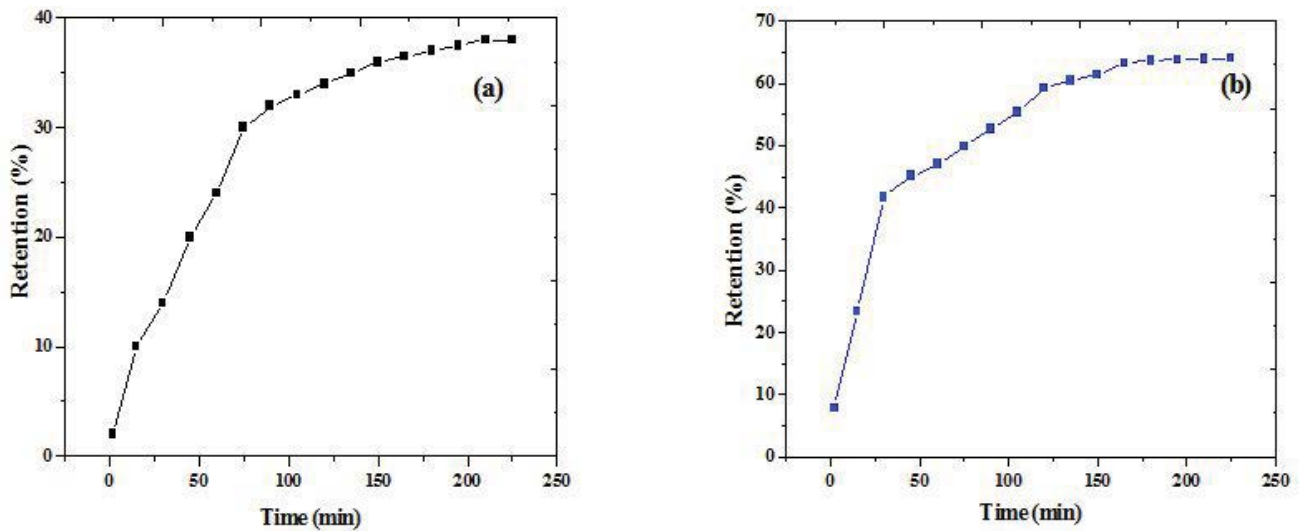


Fig. 15. EBT percentage of retention vs. filtration time on m-S (a) and m-ZX membrane (b) ($d \leq 80 \mu\text{m}$, $P = 1 \text{ bar}$).

on the zeolite membrane. Fig. 14 shows the evolution of flows as a function of filtration time. The fluxes obtained after the first 15 min are 771 and $189 \text{ Lm}^{-2}\cdot\text{h}^{-1}$ of the bare membrane support and with the zeolite layer, respectively. There is also a significant decrease of about 50% of the initial flux of the support alone and 40% for the m-ZX membrane after 3.5 h of filtration before the clogging of the two membranes. This could be attributed to the deposition of the zeolite, which reduces the size of the pores and the size of its own channels.

3.11. Retention of EBT on m-S and m-ZX membrane ($d \leq 80 \mu\text{m}$)

Fig. 15 illustrates the evolution of the percentage of EBT retention as function of the filtering time for both membranes (m-S and m-ZX). For the support, the filtration reaches a retention of 20% after 60 min, while in the same period, the composite membrane reaches a retention of 45%. The maximum retention values corresponding to saturation are 38% and 69% for m-S and m-ZX, respectively. These values were marked after a filtration period of 3.5 and 2.67 h for the first and second graphs, respectively. It should be noted that the maximum retention of m-S was achieved by the second membrane before 45 min of filtration.

4. Conclusion

In the present paper, X-type zeolite was successfully synthesized by the hydrothermal route. The verification of the obtained phase was identified by XRD, SEM/EDX analyses. In addition, membrane supports were prepared from a clay with grains' size is less than $80 \mu\text{m}$, composed essentially from kaolinite, illite, vermiculite, calcite, and quartz. The use of starch as a porogen agent, helped in increasing the porosity of support, but produced pores with less effective diameters for filtration. While the use of the zeolite layer deposited on the support and inside its pores had a significant impact on filtration. This is proven by the results of the performed analyses, which showed an improvement

of approximately 60% of the initial flux permeability and an improvement of the percentage of EBT dye retention of about 26% compared to that of the membrane support alone. Hence, the filtration method on the composite membrane based on clay and X-type zeolite can be used as an alternative ecological method to remove dyes from water environment. The mechanism that explains the behavior of the membrane during filtration could be attributed to the size of the pores and the size of the dye without neglecting the role of the adsorption of the dye on the membrane because of the difference between the charge on the membrane surface and the charge of EBT. On the other hand, an additional study will be essential to the improvement of the retention capacity of the EBT dye and of the factors influencing the retention of this dye, such as the pH and the temperature of the solution, and the choice of another type of layer to be deposited on the support.

References

- [1] H.B. Mansour, O. Boughzala, D. Dridi, D. Barillier, L. Chekir-Ghedira, R. Mosrati, Textiles dyes as a source of wastewater contamination: screening of the toxicity and treatment methods, *J. Water Sci.*, 24 (2011) 209–238.
- [2] W. Boumya, M. Khnifira, A. Machrouhi, M. Abdennouri, M. Sadiq, M. Achak, G. Serdaroğlu, S. Kaya, S. Şimşek, N. Barka, Adsorption of Eriochrome Black T on the chitin surface: experimental study, DFT calculations and molecular dynamics simulation, *J. Mol. Liq.*, 331 (2021) 115706, doi: 10.1016/j.molliq.2021.115706.
- [3] S.S. Moghaddam, M.R.A. Moghaddam, M. Arami, Coagulation/flocculation process for dye removal using sludge from water treatment plant: optimization through response surface methodology, *J. Hazard. Mater.*, 175 (2010) 651–657.
- [4] A. Elhalil, H. Tounsadi, R. Elmoubarki, F.Z. Mahjoubi, M. Farnane, M. Sadiq, M. Abdennouri, S. Qourzal, N. Barka, Factorial experimental design for the optimization of catalytic degradation of malachite green dye in aqueous solution by Fenton process, *Water Resour. Ind.*, 15 (2016) 41–48.
- [5] A. Krajňák, E. Viglašová, M. Galamboš, L. Krivosudský, Kinetics, thermodynamics and isotherm parameters of uranium(VI) adsorption on natural and HDTMA-intercalated bentonite and zeolite, *Desal. Water Treat.*, 127 (2018) 272–281.

- [6] G. Capar, U. Yetis, L. Yilmaz, Membrane based strategies for the pre-treatment of acid dye bath wastewaters, *J. Hazard. Mater.*, 135 (2006) 423–430.
- [7] S. Loera-Serna, E. Ortiz, H. Beltrán, First trial and physicochemical studies on the loading of basic fuchsin, crystal violet and Black Eriochrome T on HKUST-1, *New J. Chem.*, 41 (2017) 3097–3105.
- [8] A. Klimonda, I. Kowalska, Membrane technology for the treatment of industrial wastewater containing cationic surfactants, *Water Resour. Ind.*, 26 (2021) 100157, doi: 10.1016/j.wri.2021.100157.
- [9] L. Yu, N. Al-Jariry, T. Serikbayeva, J. Hedlund, Ultra-thin zeolite CHA and FAU membranes for desalination by pervaporation, *Sep. Purif. Technol.*, 294 (2022) 121177, doi: 10.1016/j.seppur.2022.121177.
- [10] L. Zeng, C. Gao, The prospective application of membrane distillation in the metallurgical industry, *Membr. Technol.*, 2010 (2010) 6–10.
- [11] A. Lahnafi, A. Elgamouz, N. Tijani, L. Jaber, A. Kawde, Hydrothermal synthesis and electrochemical characterization of novel zeolite membranes supported on flat porous clay-based microfiltration system and its application of heavy metals removal of synthetic wastewaters, *Microporous Mesoporous Mater.*, 334 (2022) 111778, doi: 10.1016/j.micromeso.2022.111778.
- [12] Y.J. Zhang, H. Chen, P. Yang, H.C.J. Li, Developing silica fume-based self-supported ECR-1 zeolite membrane for seawater desalination, *Mater. Lett.*, 236 (2019) 538–541.
- [13] A. Tahiri, L. Messaoudi, N. Tijani, M.H. Zerrouk, M. Messaoudi, Manufacture and characterization of flat membrane supports based on Moroccan Rif clay, *Mater. Today Proc.*, 43 (2021) 209–215.
- [14] A. El-kordy, A. Elgamouz, E.M. Lemdek, N. Tijani, S.S. Alharthi, A. Kawde, I. Shehadi, Preparation of Sodalite and Faujasite clay composite membranes and their utilization in the decontamination of dye effluents, *Membranes*, 12 (2021) 12, doi: 10.3390/membranes12010012.
- [15] A. Elgamouz, N. Tijani, I. Shehadi, K. Hasan, M.A.-F. Kawam, Characterization of the firing behaviour of an illite-kaolinite clay mineral and its potential use as membrane support, *Heliyon*, 5 (2019) e02281, doi: 10.1016/j.heliyon.2019.e02281.
- [16] Y. Dehmani, A. Ed-Dra, O. Zennouhi, A. Bouymajane, F.R. Filali, L. Nassiri, S. Abouarnadasse, Chemical characterization and adsorption of oil mill wastewater on Moroccan clay in order to be used in the agricultural field, *Heliyon*, 6 (2020) e03164, doi: 10.1016/j.heliyon.2020.e03164.
- [17] M. Messaoudi, M. Douma, N. Tijani, L. Messaoudi, Study of the permeability of tubular mineral membranes: application to wastewater treatment, *Heliyon*, 7 (2021) e06837, doi: 10.1016/j.heliyon.2021.e06837.
- [18] S. Iaich, L. Messaoudi, Preparation of new ceramic supports macro-porous for microfiltration and ultrafiltration membranes based Moroccan clay, *IOSR-J. Mech. Civ. Eng.*, 11 (2014) 56–62.
- [19] S. Bousbih, E. Errais, F. Darragi, J. Duplay, M. Trabelsi-Ayadi, M.O. Daramola, R.B. Amar, Treatment of textile wastewater using monolayered ultrafiltration ceramic membrane fabricated from natural kaolin clay, *Environ. Technol.*, 42 (2020) 1–25.
- [20] D. Yeskis, A.F.K.V. Groos, S. Guccenhetm, The dehydroxylation of kaolinite, *Am. Mineral.*, 70 (1985) 159–164.
- [21] H.A. Patel, R.S. Somani, H.C. Bajaj, R.V. Jasra, Nanoclays for polymer nanocomposites, paints, inks, greases and cosmetics formulations, drug delivery vehicle and wastewater treatment, *Bull. Mater. Sci.*, 29 (2006) 133–145.
- [22] A. Elgamouz, H. Bendifi, M. El Amame, L. Messaoudi, N. Tijani, Physico-chemical characterisation of a clay rock from Meknes-Tafilalet region, *Phys. Chem. News*, 34 (2006) 120–125.
- [23] H. Alouloua, H. Bouhamed, A. Ghorbel, R.B. Amar, S. Khemakhem, Elaboration and characterization of ceramic microfiltration membranes from natural zeolite: application to the treatment of cuttlefish effluents, *Desal. Water Treat.*, 95 (2017) 1–9.
- [24] F. Pechar, D. Rykl, Infrared spectra of natural zeolites of the stilbite group, *Chem. Zvesti.*, 35 (1981) 189–202.
- [25] A. Zainal Abidin, N.H.H. Abu Bakar, E.P. Ng, W.L. Tan, Rapid degradation of methyl orange by Ag doped zeolite X in the presence of borohydride, *J. Taibah Univ. Sci.*, 11 (2017) 1070–1079.
- [26] L.S.M. Nazir, Y.F. Yeong, T.L. Chew, Controlled growth of Faujasite zeolite with NaX topology by manipulating solution aging and Na₂O/Al₂O₃ ratios, *Colloids Surf., A*, 600 (2020) 124803, doi: 10.1016/j.colsurfa.2020.124803.
- [27] M.M. Rahman, M. Muttakin, A. Pal, A.Z. Shafiqullah, B.B. Saha, A statistical approach to determine optimal models for IUPAC-classified adsorption isotherms, *Energies*, 12 (2019) 4565, doi: 10.3390/en12234565.
- [28] M. Mouiya, A. Bouazizi, A. Abourriche, Y. El Khessaimi, A. Benhammou, Y. Elhafiane, Y. Taha, M. Oumam, Y. Abouliatim, A. Smith, H. Hannache, Effect of sintering temperature on the microstructure and mechanical behavior of porous ceramics made from clay and banana peel powder, *Results Mater.*, 4 (2019) 100028, doi: 10.1016/j.rinma.2019.100028.

Supporting information

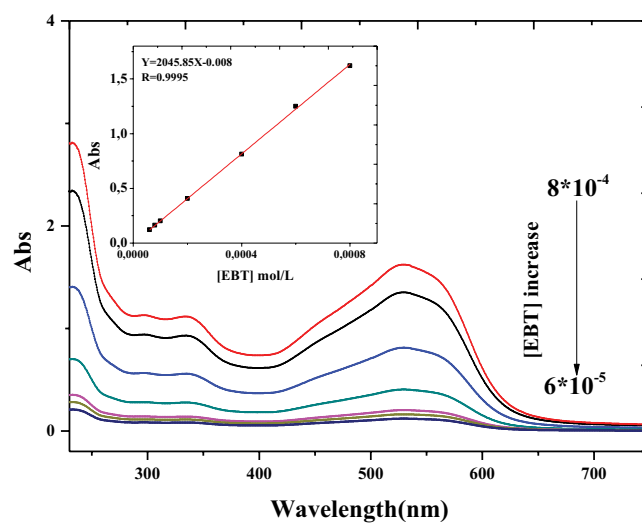


Fig. S1. UV-visible spectra of Eriochrome Black T solutions, with calibration curve.